Microfluid Nanofluid (2017) 21:133
DOI 10.1007/s10404-017-1967-7

RESEARCH PAPER

Size-dependent vibration analysis of multi-span functionally graded material micropipes conveying fluid using a hybrid method

Jiaquan Deng[1] · **Yongshou Liu**[1] · **Wei Liu**[1]

Received: 4 May 2017 / Accepted: 11 July 2017 / Published online: 21 July 2017

Abstract Microscale fluid-conveying pipes and functionally graded materials (FGMs) have many potential applications in engineering fields. In this paper, the free vibration and stability of multi-span FGM micropipes conveying fluid are investigated. The material properties of FGM micropipes are assumed to change continuously through thickness direction according to a power law. Based on modified couple stress theory, the governing equation and boundary conditions are derived by applying Hamilton's principle. Subsequently, a hybrid method which combines reverberation-ray matrix method and wave propagation method is developed to determine the natural frequencies, and the results determined by present method are compared with those in the existing literature. Then, the effects of material length scale parameter, volume fraction exponent, location and number of supports on dynamic characteristics of multi-span FGM micropipes conveying fluid are discussed. The results show that the size effect is significant when the diameter of micropipe is comparable to the length scale parameter, and the natural frequencies determined by modified couple stress theory are larger than those obtained by classical beam theory. It is also found that natural frequencies and critical velocities increase rapidly with the increase of volume fraction exponent when it is less than 10, and the intermediate supports could improve the stability of pipes conveying fluid significantly.

✉ Yongshou Liu
yongshouliu@nwpu.edu.cn

1 Department of Engineering Mechanics, Northwestern Polytechnical University, Xi'an, People's Republic of China

Keywords Size-dependent vibration · Functionally graded materials · Multi-span micropipes conveying fluid · Hybrid method

1 Introduction

Functionally graded materials (FGMs) can be described as inhomogeneous composites that have a smooth and continuous variation of material properties from one surface to the other. Compared with traditional composite materials, FGMs possess a number of advantages including enhanced thermal resistance, improved residual stress distribution, higher fracture toughness and inferior stress intensity factors (Birman and Byrd 2007). Another important feature of FGMs is the designability. The gradual variation of material properties can be tailored to suit special purposes in engineering applications. It is not surprising that the FGMs have received considerable attention in many engineering fields, such as aerospace, electronics, biomedical implants and nuclear plants (Jha et al. 2013; Wang and Zu 2017).

Being the simplest form of fluid–structure interaction problem, the dynamics of pipes conveying fluid has attracted enormous considerations from researchers due to the interesting dynamic behavior and wide engineering applications (Wang et al. 2012). Numerous works have been carried out on vibration and stability of pipes conveying fluid (Ibrahim 2010, 2011; Li et al. 2015; Païdoussis 2014; Païdoussis and Li 1993). Although many aspects of this problem have been investigated in past decades, most of the papers are limited to the model of single-span pipes conveying fluid. Arbitrary multi-span piping systems, which are thought to match with realistic situation in engineering applications that intermediate supports are more frequently to be installed, have been paid less attention until now. The main reason is that the classical mode method is easily applicable to the special cases where the functions for the mode shapes are obtainable, such as single-span or periodical multi-span pipes (Wu and Shih 2001). Wu and Shih (2001) proposed a "numerical" mode method to investigate the dynamic characteristics of a multi-span pipe conveying fluid. However, this "numerical" mode method applied mode shapes of pipe with stationary fluid to calculate natural frequencies of pipes with flowing fluid. Deng et al. (2016) applied the dynamic stiffness method (DSM) to determine the frequency responses of a multi-span pipe conveying fluid subjected to a transient load. Li et al. (2012a) employed the reverberation matrix method and fast Fourier transform to investigate the transient responses of a multi-span pipe conveying fluid. They reported that a reliable and accurate method developed for dynamic analysis of arbitrary multi-span pipes conveying fluid is important in engineering fields.

On the other hand, due to the recent technological developments in science and materials, both FGMs and fluid-conveying pipes have been made in micro- and nanoscales. Micro- and nanoscaled FGMs are used in microelectromechanical systems (MEMS) (Fu et al. 2004), nanoelectromechanical systems (NEMS) (Lee et al. 2006), ultra-thin films (Lü et al. 2009), microsensors and microactuators (Salamat-talab et al. 2012). And fluid-conveying micropipes have wide applications in microfluidic devices (Amiri et al. 2016), fluid filtration devices (Wang et al. 2013) and target drug delivery devices (Wu et al. 2011). The fluid-conveying micropipes also have been utilized to measure the fluid density, viscosity and chemical concentration (Enoksson et al. 1997; Najmzadeh et al. 2007). Therefore, understanding the vibrational characteristics of structures at micro- and nanoscales is of practical importance in many present and potential applications. However, it should be mentioned that the classical continuum theory is unable to predict the size-dependent behavior which has been observed in experimental investigations (Fleck et al. 1994; Lam et al. 2003). To overcome this problem, several size-dependent nonclassical continuum theories including couple stress theory (Toupin 1962), strain gradient theory (Mindlin and Eshel 1968), nonlocal elasticity theory (Eringen 1972), surface elasticity theory (Gurtin and Murdoch 1975), modified couple stress theory (Yang et al. 2002), modified strain gradient theory (Lam et al. 2003) and nonlocal strain gradient theory (Lim et al. 2015) have been proposed to capture the size effect.

Based on these nonclassical continuum theories, numerous models have been developed to study the size-dependent dynamic behaviors of FGM structures (Aghazadeh et al. 2014; Ke et al. 2012; Komijani et al. 2014; Li and Hu 2017a, b; Li et al. 2016a; Nateghi and Salamat-talab 2013; Reddy 2011; Simsek and Reddy 2013) and fluid-conveying pipes (Li and Hu 2016a; Rinaldi et al. 2010; Wang 2010; Yang et al. 2014; Zhang et al. 2013, 2015) at micro- or nanoscales. However, the studies concerned with FGM pipes conveying fluid are limited (Chen and Su 2017; Deng et al. 2016; Sheng and Wang 2008, 2010; Wang and Liu 2016). And the literature related to size-dependent dynamics of FGM pipes conveying fluid at micro- or nanoscales is fewer. Setoodeh and Afrahim (2014) studied the free vibration of a simply supported FGM micropipe conveying fluid by strain gradient theory. Ansari et al. (2015, 2016a) studied the size-dependent free vibration of fluid-conveying FGM shells through strain gradient theory. Filiz and Aydogdu (2015) analyzed the wave propagation in a coupled FGM nanotube conveying fluid by nonlocal elasticity theory. It could be expected that the size-dependent dynamics of FGM pipes conveying fluid will attract more interest in future.

As mentioned earlier, a reliable and accurate method developed for dynamics of arbitrary multi-span pipes conveying fluid is significant in engineering applications. Recently, Pao et al. (1999) and Howard and Pao (1998) proposed a method of reverberation-ray matrix (MRRM), which is used to investigate the elastic wave transmission in planar trusses. Subsequently, Pao and Chen (2009) extended this method to space frames. Tian and Xie (2009) developed this method to investigate the wave propagation in multilayered solids. Miao et al. (2013) employed this method to predict the transient responses of laminated composite beams. Ma et al. (2016) adopted this method to analyze the dispersion of Lamb waves in composite laminates. As reported by Pao et al. (1999), the MRRM is particularly suitable for multi-branched structures. On the other hand, the wave propagation method has been used to study the dynamics of single-span pipes conveying fluid (Li et al. 2012b; Zhang 2002; Zhang et al. 2014).

In this paper, the size-dependent free vibration and stability of multi-span FGM micropipes conveying fluid are investigated. The governing equation and boundary conditions are derived by modified couple stress theory and Hamilton's principle. A hybrid method which combines the MRRM and the wave propagation method is developed to determine the natural frequencies of multi-span pipes conveying fluid. The results calculated by the hybrid method are compared with those in the existing literature to verify the present method, and then, the effects of material length scale parameter, volume fraction exponent, location and number of supports on free vibration and stability of FGM micropipes conveying fluid are discussed in detail.

2 Material properties of the FGM micropipes

A FGM micropipe conveying fluid with length L, constant fluid velocity U and mean radius R is shown in Fig. 1. R_i and R_o represent the inner and outer radii, respectively. Displacement components in x, y and z directions are u, v and w, respectively. It is assumed that the micropipe is slender, and the fluid is incompressible, inviscid and irrotational. To model the internal flow, a continuum-based plug flow is adopted in which the fluid is considered as an infinitely flexible rodlike structure flowing through the micropipe (Ansari et al. 2016b; Li et al. 2016b). It is worth noting that the fluid velocity profile in cross section may be nonuniform due to the microscale. However, based on the investigation of Guo et al. (2010), the plug flow is an acceptable model for the internal fluid in the micropipe.

The material properties of the pipe are considered to vary continuously along the thickness direction according to a power law, and effective material properties can be written as

$$E = V_i E_i + V_o E_o \tag{1}$$

$$\mu = V_i \mu_i + V_o \mu_o \tag{2}$$

$$\rho = V_i \rho_i + V_o \rho_o \tag{3}$$

where E, μ and ρ are Young's modulus, shear modulus and density of the FGM micropipe, respectively. The Poisson's ratio ν is assumed to be a constant (Reddy 2011). Subscripts i and o represent the inner and outer surfaces, respectively. The volume fractions of materials can be given as (Setoodeh and Afrahim 2014; Shen et al. 2016)

$$V_i = \left(\frac{R_o - r}{R_o - R_i}\right)^n, \quad V_o = 1 - V_i \tag{4}$$

where r is the radius of a reference point and superscript n is the volume fraction exponent which characterizes the volume fraction profile of the constituent materials.

The variation of volume fraction V_i with thickness direction for various values of volume fraction exponents n is depicted in Fig. 2. It can be seen from Fig. 2 that when the exponent n is assumed to be zero, the FGM micropipe reduces to homogeneous micropipe.

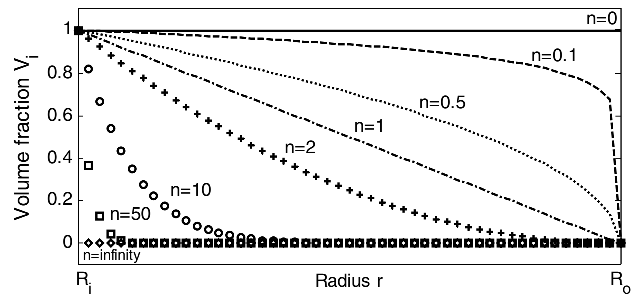

Fig. 2 Variation of volume fraction V_i with thickness direction

3 Mathematical formulations

3.1 Modified couple stress theory

The modified couple stress theory presented by Yang et al. (2002) results from the classical couple stress theory (Toupin 1962). Two advantages of modified couple stress theory over classical couple stress theory are the inclusion of asymmetric couple stress tensor and the introduction of only one length scale parameter (Reddy 2011). For more details on this theory, the interested reader can refer to Yang et al. (2002) and Reddy (2011).

According to the modified couple stress theory, the total strain energy of structures is a function of both strain tensor (conjugated with stress tensor) and curvature tensor (conjugated with couple stress tensor). And the strain energy U_m can be written as (Reddy 2011; Yang et al. 2002)

$$U_m = \frac{1}{2}\int_{\Omega} (\boldsymbol{\sigma}:\boldsymbol{\varepsilon} + \mathbf{m}:\boldsymbol{\chi})\mathrm{d}V \tag{5}$$

where U_m is the strain energy, Ω is the volume, $\boldsymbol{\sigma}$ is the stress tensor, $\boldsymbol{\varepsilon}$ is the strain tensor, $\mathbf{m}$ is deviatoric part of the symmetric couple stress tensor and $\boldsymbol{\chi}$ is symmetric curvature tensor. And these tensors can be written as

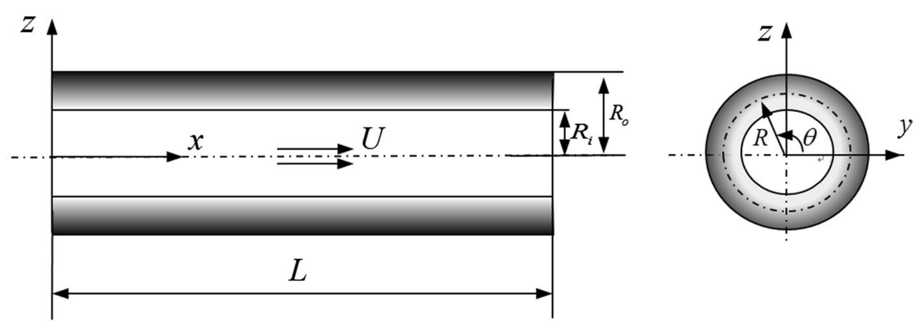

Fig. 1 A schematic model of a FGM micropipe conveying fluid

$$\boldsymbol{\sigma} = \lambda \mathrm{tr}(\boldsymbol{\varepsilon})\mathbf{I} + 2\mu\boldsymbol{\varepsilon} \tag{6}$$

$$\boldsymbol{\varepsilon} = \frac{1}{2}\left[\nabla\mathbf{u} + (\nabla\mathbf{u})^T\right] \tag{7}$$

$$\mathbf{m} = 2l^2\mu\boldsymbol{\chi} \tag{8}$$

$$\boldsymbol{\chi} = \frac{1}{2}\left[\nabla\boldsymbol{\theta} + (\nabla\boldsymbol{\theta})^T\right] \tag{9}$$

where $\mathbf{u}$ is the displacement vector, $\boldsymbol{\theta}$ is the rotation vector, l is material length scale parameter and λ and μ are the Láme's constants. To simplify the analysis, the material length scale parameter l is assumed to be a constant in this paper (Ansari et al. 2015; Ke et al. 2012; Salamat-talab et al. 2012; Simsek and Reddy 2013). And the rotation vector $\boldsymbol{\theta}$ can be written as

$$\boldsymbol{\theta} = \frac{1}{2}\mathrm{curl}\,\mathbf{u} \tag{10}$$

According to the Euler–Bernoulli beam theory, the displacement field of an arbitrary point along the x-, y- and z-axes (shown in Fig. 1) can be expressed as

$$u = u_0 - z\psi(x,\ t), \quad v = 0, \quad w = w(x,\ t) \tag{11}$$

where $\psi(x, t)$ is the rotation of pipe cross section. u_0 and w are the axial and transverse displacements on the mid-axis, respectively. In view of the small deformations assumption, the longitudinal displacement may be expressed as following form by neglecting the axial deformation (Li et al. 2016b)

$$u = -z\psi(x,\ t) \tag{12}$$

and the rotation can be written as

$$\psi(x) \approx w(x)' \tag{13}$$

where the primes represent differentiation with respect to x. Substituting Eqs. (11), (12) and (13) into Eq. (7), the only one nonzero strain component can be obtained (Yang et al. 2014)

$$\varepsilon_{xx} = -zw'' \tag{14}$$

Substituting Eqs. (11), (12) and (13) into Eq. (10) yields

$$\theta_y = -w', \quad \theta_x = \theta_z = 0 \tag{15}$$

Substituting Eq. (15) into Eq. (9), following equations can be obtained

$$\chi_{xy} = -\frac{1}{2}w'', \quad \chi_{xx} = \chi_{yy} = \chi_{zz} = \chi_{yz} = \chi_{zx} = 0 \tag{16}$$

3.2 Governing equation and boundary conditions of FGM micropipes conveying fluid

In this section, the equations of motion for the size-dependent FGM micropipes conveying fluid will be built by modified couple stress theory and Hamilton's principle. In general, the main assumptions and simplifications for the equations of FGM micropipes conveying fluid are outlined as follows:

1. The material properties of FGM micropipes are assumed to change continuously through thickness direction according to a power law;
2. The Euler–Bernoulli beam theory is adopted to model the pipe, and the deformations are assumed to be small;
3. The strain energy of the FGM micropipe obeys the modified couple stress theory;
4. The material length scale parameter l in FGM micropipes is assumed to be a constant;
5. The internal flow in the micropipe is assumed to be a steady plug flow.

Substituting Eq. (14) to (6) and neglecting the Poisson's effect, the components of stress of the FGM micropipe can be obtained (Asghari et al. 2010; Nateghi and Salamat-talab 2013)

$$\sigma_{xx} = -Ezw'', \quad \sigma_{yy} = \sigma_{zz} = \sigma_{xy} = \sigma_{yz} = \sigma_{zx} = 0 \tag{17}$$

where E is Young's modulus of the FGM micropipe, which is the function of position.

Substitution of Eq. (16) into (8) gives

$$m_{xy} = -\mu l^2 w'', \quad m_{xx} = m_{yy} = m_{zz} = m_{yz} = m_{zx} = 0 \tag{18}$$

The strain energy of the FGM micropipe can be written as

$$U_{\mathrm{m}} = \frac{1}{2}\int_L\int_A \left(Ez^2 + \mu l^2\right)w''^2 \mathrm{d}A\mathrm{d}x \tag{19}$$

and Eq. (19) can be rewritten as (Asghari et al. 2010)

$$U_{\mathrm{m}} = \frac{1}{2}\int_L \left[(EI)^* + (\mu A)^* l^2\right] w''^2 \mathrm{d}x \tag{20}$$

where

$$(EI)^* = \int_A Ez^2 \mathrm{d}A = \int_0^{2\pi}\int_{R_i}^{R_o} E(r)r^2 \sin^2\theta r\mathrm{d}r\mathrm{d}\theta \tag{21}$$

and

$$(\mu A)^* = \int_A \mu \mathrm{d}A = \int_0^{2\pi}\int_{R_i}^{R_o} \mu(r) r\mathrm{d}r\mathrm{d}\theta \tag{22}$$

The kinetic energy of the pipe can be expressed as

$$T_{\mathrm{p}} = \frac{1}{2}m_{\mathrm{p}}^*\int_L \dot{w}^2 \mathrm{d}x \tag{23}$$

where the over-dot represents differentiation with respect to time t and the equivalent mass m_{p}^* of per unit length of the FGM pipe can be defined as (Asghari et al. 2010)

$$m_{\mathrm{p}}^{*}=\int_{A}\rho\mathrm{d}A=\int_{0}^{2\pi}\int_{R_{\mathrm{i}}}^{R_{\mathrm{o}}}\rho(r)r\mathrm{d}r\mathrm{d}\theta \tag{24}$$

The kinetic energy of the internal flow can be written as (Païdoussis 2014)

$$T_{\mathrm{f}}=\frac{1}{2}M_{\mathrm{f}}\int_{L}\left[\left(\dot{w}+Uw'\right)^{2}+U^{2}\right]\mathrm{d}x \tag{25}$$

where M_{f} is the mass of fluid per unit length. According to Paidoussis (2014), the statement of Hamilton's principle for fully supported pipes conveying fluid can be written as

$$\delta\int_{t_1}^{t_2}l_c\mathrm{d}t=0 \tag{26}$$

where $l_{\mathrm{c}} = T_{\mathrm{p}} + T_{\mathrm{f}} - U_{\mathrm{m}}$ is the Lagrangian of the system. Substituting Eqs. (20), (23) and (25) into Eq. (26) and applying the variational techniques to Eq. (26), the governing equation of the FGM micropipe conveying fluid can be obtained.

$$\left[(EI)^{*}+(\mu A)^{*}l^{2}\right]w''''+M_{\mathrm{f}}U^{2}w''+2M_{\mathrm{f}}U\dot{w}'+\left(M_{\mathrm{f}}+m_{\mathrm{p}}^{*}\right)\ddot{w}=0 \tag{27}$$

It should be noted that gravity, damping, externally imposed tension and pressurization effects are neglected in above equation. And the boundary conditions for a micropipe with both ends simply supported can be expressed as

$$w(0,\ t)=w''(0,\ t)=0,\quad w(L,\ t)=w''(L,\ t)=0 \tag{28}$$

Compared with governing equation of homogeneous micropipes conveying fluid based on the modified couple stress theory (Wang 2010), the flexural rigidity and the mass of the pipe are replaced by equivalent flexural rigidity $[(EI)^{*} + (\mu A)^{*}l^{2}]$ and the equivalent mass m_{p}^{*} of per unit length of the FGM micropipe.

4 Hybrid method for multi-span pipes conveying fluid

In this section, the MRRM combined with the wave propagation method is developed to build the characteristic equation of arbitrary multi-span FGM micropipes conveying fluid.

The general solution for Eq. (27) can be expressed as (Li and Hu 2016b)

$$w(x,\ t)=\hat{w}(x,\ \omega)e^{i\omega t} \tag{29}$$

where ω is the circular frequency and $i=\sqrt{-1}$.

Substituting Eq. (29) into (27) yields

$$\left[(EI)^{*}+(\mu A)^{*}l^{2}\right]\hat{w}''''+M_{\mathrm{f}}U^{2}\hat{w}''+i2\omega M_{\mathrm{f}}U\hat{w}'-\omega^{2}\left(M_{\mathrm{f}}+m_{\mathrm{p}}^{*}\right)\hat{w}=0 \tag{30}$$

The displacement in frequency domain can be set as

$$\hat{w}=ce^{ikx} \tag{31}$$

where c is a constant. Substituting Eq. (31) into Eq. (30) yields

$$\left[(EI)^{*}+(\mu A)^{*}l^{2}\right]k^{4}-M_{\mathrm{f}}U^{2}k^{2}-2\omega M_{\mathrm{f}}Uk-\omega^{2}\left(M_{\mathrm{f}}+m_{\mathrm{p}}^{*}\right)=0 \tag{32}$$

It should be mentioned that the wavenumber k in Eq. (32) has four roots k_1, k_2, k_3 and k_4 which correspond to four wave modes. According to MRRM, the wave modes can be divided into arriving and departing waves (Pao et al. 1999). And in wave propagation method, the waves can be divided into positive- and negative-traveling waves (Lee et al. 2007; Zhang et al. 2014). Then, the transverse displacement in frequency domain can be rewritten as

$$\hat{w}=\sum_{j=1}^{4}w_{j}e^{ik_{j}x} \tag{33}$$

Accordingly, the rotation $\hat{\theta}$, bending moment $\hat{M}$ and shear force $\hat{Q}$ in frequency domain can be written as

$$\hat{\theta}=\sum_{j=1}^{4}ik_{j}w_{j}e^{ik_{j}x} \tag{34}$$

$$\hat{M}=\sum_{j=1}^{4}\left[(EI)^{*}+(\mu A)^{*}l^{2}\right]k_{j}^{2}w_{j}e^{ik_{j}x} \tag{35}$$

$$\hat{Q}=\sum_{j=1}^{4}\left[(EI)^{*}+(\mu A)^{*}l^{2}\right]ik_{j}^{3}w_{j}e^{ik_{j}x} \tag{36}$$

4.1 Application of MRRM

Based on MRRM, continuity conditions of displacements and equilibrium conditions of forces at each node of the multi-span micropipe are used to build the scattering matrix. Dual superscripts w_j^{JK} ($j = 1, 2, 3, 4$) are introduced to describe the arriving and departing waves (Miao et al. 2013; Pao et al. 1999). Superscripts J and K indicate adjacent nodes. It should be mentioned that in arriving waves, w_j^{JK} represents the arriving wave from node K to node J, while in departing waves, w_j^{JK} denotes the departing wave from node J to node K.

The wave motions in a typical multi-span FGM micropipe conveying fluid are shown in Fig. 3. Based on MRRM, the arriving and departing waves at each node can be listed as

$$\mathbf{a}^1 = \left(w_1^{12}, w_2^{12}\right)^T, \mathbf{a}^2 = \left(w_3^{21}, w_4^{21}, w_1^{23}, w_2^{23}\right)^T, \ldots, \\ \mathbf{a}^n = \left(w_3^{n(n-1)}, w_4^{n(n-1)}\right)^T \tag{37}$$

$$\mathbf{d}^1 = \left(w_3^{12}, w_4^{12}\right)^T, \mathbf{d}^2 = \left(w_1^{21}, w_2^{21}, w_3^{23}, w_4^{23}\right)^T, \ldots, \\ \mathbf{d}^n = \left(w_1^{n(n-1)}, w_2^{n(n-1)}\right)^T \tag{38}$$

in which $\mathbf{a}$ and $\mathbf{d}$ are the arriving and departing waves, respectively. It should be noted that superscripts 1, 2,…, n represent the node numbers, while subscripts 1, 2, 3, 4 correspond to k_1, k_2, k_3 and k_4.

According to Pao et al. (1999), the global scattering relation can be written in following form

$$\mathbf{d} = \mathbf{S}\mathbf{a} + \mathbf{s} \tag{39}$$

in which $\mathbf{S}$ is the global scattering matrix and $\mathbf{s}$ is the global source vector. If there is no external force applied at the piping system, the global source vector $\boldsymbol{s} = \mathbf{0}$. The global scattering matrix $\mathbf{S}$ can be built by assembling the local scattering matrix at each node, and the local scattering matrix can be obtained by continuity conditions of displacements and equilibrium conditions of forces at each node. For instance, boundary conditions at node 1 can be written as

$$\hat{w}^1 = 0, \quad \hat{M}^1 = 0 \tag{40}$$

Substituting Eqs. (33) and (35) into Eq. (40) gives

$$w_1^{12} + w_2^{12} + w_3^{12} + w_4^{12} = 0 \tag{41}$$

$$\beta_1 w_1^{12} + \beta_2 w_2^{12} + \beta_3 w_3^{12} + \beta_4 w_4^{12} = 0 \tag{42}$$

where $\beta_j = [(EI)^* + (\mu A)^* l^2]k_j^2$. Recalling that the arriving and departing waves at node 1 are

$$\mathbf{a}^1 = \left(w_1^{12}, w_2^{12}\right)^T, \quad \mathbf{d}^1 = \left(w_3^{12}, w_4^{12}\right)^T \tag{43}$$

Then, Eqs. (41) and (42) can be rewritten in matrix form

$$\begin{bmatrix} 1 & 1 \\ \beta_1 & \beta_2 \end{bmatrix} \mathbf{a}^1 + \begin{bmatrix} 1 & 1 \\ \beta_3 & \beta_4 \end{bmatrix} \mathbf{d}^1 = 0 \tag{44}$$

The local scattering relation at node 1 can be written as (Pao et al. 1999)

$$\mathbf{d}^1 = \mathbf{S}^1 \mathbf{a}^1 \tag{45}$$

in which $\mathbf{S}^1$ is local scattering matrix of node 1. Combining Eqs. (44) and (45), the local scattering matrix can be expressed as

$$\mathbf{S}^1 = -\begin{bmatrix} 1 & 1 \\ \beta_3 & \beta_4 \end{bmatrix}^{-1} \cdot \begin{bmatrix} 1 & 1 \\ \beta_1 & \beta_2 \end{bmatrix} \tag{46}$$

The local scattering matrix of node 2 can be established by the continuity and equilibrium conditions, which can be written as (Harland et al. 2001; Lee et al. 2007; Tan and Kang 1998)

$$\hat{w}_-^2 = 0, \quad \hat{w}_+^2 = 0, \quad \hat{\varphi}_-^2 = \hat{\varphi}_+^2, \quad \hat{M}_+^2 - \hat{M}_-^2 = 0 \tag{47}$$

where subscripts "−, +" represent the left and right sides of a node, respectively. And recalling that the arriving and departing waves at node 2 are

$$\mathbf{a}^2 = \left(w_3^{21}, w_4^{21}, w_1^{23}, w_2^{23}\right)^T, \quad \mathbf{d}^2 = \left(w_1^{21}, w_2^{21}, w_3^{23}, w_4^{23}\right)^T \tag{48}$$

After some manipulations, the local scattering matrix of node 2 can be built

$$\mathbf{S}^2 = -\begin{bmatrix} 1 & 1 & 0 & 0 \\ 0 & 0 & 1 & 1 \\ \lambda_1 & \lambda_2 & -\lambda_3 & -\lambda_4 \\ \beta_1 & \beta_2 & -\beta_3 & -\beta_4 \end{bmatrix}^{-1} \cdot \begin{bmatrix} 1 & 1 & 0 & 0 \\ 0 & 0 & 1 & 1 \\ \lambda_3 & \lambda_4 & -\lambda_1 & -\lambda_2 \\ \beta_3 & \beta_4 & -\beta_1 & -\beta_2 \end{bmatrix} \tag{49}$$

where $\lambda_j = ik_j$. Similarly, the local scattering matrices of other intermediate supports can be obtained by the same way.

For node n, the boundary conditions can be listed as

$$\hat{w}^n = 0, \quad \hat{M}^n = 0 \tag{50}$$

and the arriving and departing waves at node n are

$$\mathbf{a}^n = \left(w_3^{n(n-1)}, \ w_4^{n(n-1)}\right)^T, \quad \mathbf{d}^n = \left(w_1^{n(n-1)}, \ w_2^{n(n-1)}\right)^T \tag{51}$$

After some manipulations, scattering matrix of node n can be obtained

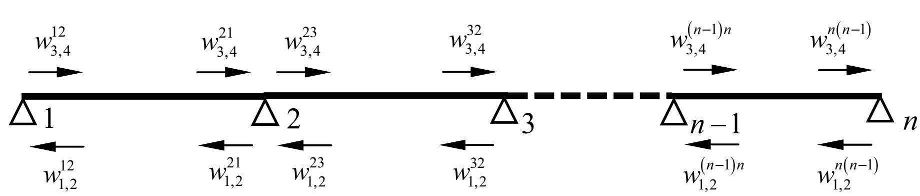

Fig. 3 Wave motions of a multi-span FGM micropipe conveying fluid

$$\mathbf{S}^n = -\begin{bmatrix} 1 & 1 \\ \beta_1 & \beta_2 \end{bmatrix}^{-1} \cdot \begin{bmatrix} 1 & 1 \\ \beta_3 & \beta_4 \end{bmatrix} \tag{52}$$

By assembling local scattering matrices, the global scattering matrix **S** of the multi-span micropipe can be obtained

$$\mathbf{S} = \mathrm{diag}\left[\mathbf{S}^1, \mathbf{S}^2, \ldots, \mathbf{S}^n\right] \tag{53}$$

In above discussions, the multi-span pipeline is assumed to be simply supported. It should be mentioned that this method also can be used to solve the pipe with other support conditions by changing the continuity and equilibrium conditions or the boundary conditions.

4.2 Application of wave propagation method

Based on wave propagation method, the wave propagation relations in sub-span element are established in this section.

The wave propagations in mth span element are shown in Fig. 4. As mentioned in the foregoing, the waves can be divided into positive- and negative-traveling waves in wave propagation method. Without loss of generality, subscripts 1, 2 in $w_j^{JK}(j = 1, 2, 3, 4)$ denote the negative-traveling waves, while subscripts 3, 4 the positive-traveling waves in this paper. The relationship between negative-traveling waves in mth span element can be written as (Lee et al. 2007; Zhang et al. 2014)

$$\mathbf{W}_{1,2}^{m(m+1)} = \mathbf{T}_{mL}\mathbf{W}_{1,2}^{(m+1)m} \tag{54}$$

in which $\mathbf{T}_{mL}$ is the left propagation matrix of mth span element and

$$\mathbf{W}_{1,2}^{m(m+1)} = \begin{Bmatrix} w_1^{m(m+1)} \\ w_2^{m(m+1)} \end{Bmatrix}, \quad \mathbf{T}_{mL} = \begin{bmatrix} e^{-ik_1 l_m} & 0 \\ 0 & e^{-ik_2 l_m} \end{bmatrix},$$
$$\mathbf{W}_{1,2}^{(m+1)m} = \begin{Bmatrix} w_1^{(m+1)m} \\ w_2^{(m+1)m} \end{Bmatrix} \tag{55}$$

Similarly, the relationship between positive-traveling waves can be expressed as

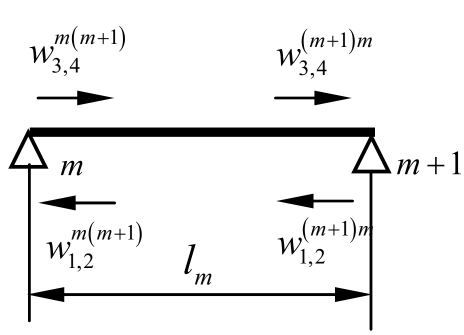

Fig. 4 Wave propagations of the mth span element

$$\mathbf{W}_{3,4}^{(m+1)m} = \mathbf{T}_{mR}\mathbf{W}_{3,4}^{m(m+1)} \tag{56}$$

in which $\mathbf{T}_{mR}$ is the right propagation matrix of mth span element and

$$\mathbf{W}_{3,4}^{(m+1)m} = \begin{Bmatrix} w_3^{(m+1)m} \\ w_4^{(m+1)m} \end{Bmatrix}, \quad \mathbf{T}_{mR} = \begin{bmatrix} e^{ik_3 l_m} & 0 \\ 0 & e^{ik_4 l_m} \end{bmatrix},$$
$$\mathbf{W}_{3,4}^{m(m+1)} = \begin{Bmatrix} w_3^{m(m+1)} \\ w_4^{m(m+1)} \end{Bmatrix} \tag{57}$$

Analogously, the local propagation matrices of other elements can be obtained by the same way.

4.3 Application of the hybrid method

In what follows, the MRRM integrating the wave propagation method is developed to build the characteristic equation. The arriving and departing waves are introduced to wave propagation matrix, and combining Eqs. (54) and (56), following matrix form can be obtained

$$\begin{Bmatrix} \mathbf{a}^m \\ \mathbf{a}^{m+1} \end{Bmatrix} = \begin{bmatrix} \mathbf{T}_{mL} & \mathbf{0} \\ \mathbf{0} & \mathbf{T}_{mR} \end{bmatrix} \begin{bmatrix} \mathbf{0} & \mathbf{I}_{2\times 2} \\ \mathbf{I}_{2\times 2} & \mathbf{0} \end{bmatrix} \begin{Bmatrix} \mathbf{d}^m \\ \mathbf{d}^{m+1} \end{Bmatrix} \tag{58}$$

where arriving and departing waves at nodes m and $m + 1$ are given by

$$\mathbf{a}^m = \left(w_1^{m(m+1)}, w_2^{m(m+1)}\right)^T, \quad \mathbf{a}^{m+1} = \left(w_3^{(m+1)m}, w_4^{(m+1)m}\right)^T \tag{59}$$

$$\mathbf{d}^m = \left(w_3^{m(m+1)}, w_4^{m(m+1)}\right)^T, \quad \mathbf{d}^{m+1} = \left(w_1^{(m+1)m}, w_2^{(m+1)m}\right)^T \tag{60}$$

Assembling the local propagation matrices, the second relationship between the arriving and departing waves can be expressed as

$$\mathbf{a} = \mathbf{PUd} \tag{61}$$

where

$$\mathbf{P} = \mathrm{diag}\left[\mathbf{T}_1, \mathbf{T}_2, \ldots, \mathbf{T}_{n-1}\right], \quad \mathbf{T}_q = \begin{bmatrix} \mathbf{T}_{qL} & \mathbf{0} \\ \mathbf{0} & \mathbf{T}_{qR} \end{bmatrix}$$
$$(q = 1,\ 2, \ldots,\ n-1) \tag{62}$$

$$\mathbf{U} = \mathrm{diag}[\mathbf{u},\ \mathbf{u}, \ldots,\ \mathbf{u}], \quad \mathbf{u} = \begin{bmatrix} \mathbf{0}_{2\times 2} & \mathbf{I}_{2\times 2} \\ \mathbf{I}_{2\times 2} & \mathbf{0}_{2\times 2} \end{bmatrix} \tag{63}$$

Combining Eqs. (39) and (61) yields

$$(\mathbf{I} - \mathbf{R})\mathbf{d} = \mathbf{s} \tag{64}$$

where, $\mathbf{R} = \mathbf{SPU}$ is the reverberation-ray matrix of structures (Pao et al. 1999). Natural frequencies of the multi-span FGM micropipe conveying fluid can be computed numerically by setting the determinant of coefficient matrix to zero

Fig. 5 A two-span FGM pipe conveying fluid

Table 1 Material properties of constituents of the FGM pipe (Deng et al. 2016)

Materials	ρ_p(kg/m^3)	E (GPa)	μ (GPa)
SiC	3210	440	188
Ti-6Al-4 V	4515	115	44.57

$$\det[\mathbf{I}-\mathbf{R}]=0 \tag{65}$$

To compute the roots of Eq. (65), one may plot the determinant with respect to frequency ω, and the detailed procedures of determining the natural frequency can be found in Deng et al. (2017a). It is worth mentioning that as pointed out by Guo and Chen (2007), the MRRM shows high accuracy, lower computational cost and uniformity of formulation in dynamic analysis of multi-branched structures. On the other hand, the wave propagation method is convenient for dynamics of pipes conveying fluid (Zhang et al. 2014), and the formulation can be formed with only one element for each sub-span. The present hybrid method inherits the advantages of both methods, and it is particularly suitable for dynamic analysis of multi-span pipes conveying fluid by using only a small number of elements.

5 Results and discussions

5.1 Verification of present analysis

To verify the present hybrid method for dynamic analysis of multi-span FGM pipes conveying fluid, natural frequencies of a two-span macroscopic FGM pipe conveying fluid are calculated and compared with those obtained by DSM (Deng et al. 2016). The model is shown in Fig. 5, and the whole pipe is simply supported by three hinged joints. The corresponding mechanical properties of the FGM pipe are listed in Table 1.

The geometrical parameters of the pipe are $R_o = 50$ mm, $R_i = 48$ mm and $L = 10$ m. The density of fluid is 1000 kg/m^3. To make the results directly comparable, dimensionless fluid velocity and natural frequency defined in Deng et al. (2016) are used

$$u=\left(\frac{M_f}{EI}\right)^{1/2}LU, \quad \varpi=\left(\frac{M_f+m}{EI}\right)^{1/2}L^2\omega \tag{66}$$

in which u is dimensionless fluid velocity and ϖ is dimensionless natural frequency. Comparisons of natural frequencies determined by present method and those calculated by DSM and FEM (Deng et al. 2016) are listed in Table 2.

Comparisons of present natural frequencies and those in Deng et al. (2016) are listed in Table 2. As expected, a good agreement is given in Table 2. The maximum relative error between present results and those obtained by DSM is 0.03%, and the maximum relative error between present results and those determined by FEM is 0.94%. This indicates that the present hybrid method is accurate for predicting the natural frequencies of multi-span FGM pipes conveying fluid.

To verify the present method for dynamic analysis of micropipes conveying fluid, fundamental natural frequencies of a pinned–pinned homogeneous micropipe conveying fluid are calculated and compared with the results obtained by differential quadrature method (DQM) (Wang 2010). The material properties of the micropipe are $E = 1.44$ GPa, $\nu = 0.38$, $l = 17.6$ μm and $\rho_p = \rho_f = 1000$ kg/m^3. And the geometrical parameters of the pipe are $D_i/D_o = 0.8$ and $L/D_o = 20$. The parameters D_i and D_o represent the inner and outer diameters of the micropipe, respectively.

Table 2 Comparisons of natural frequencies of the two-span FGM pipe conveying fluid

U	Results	Exponent $n = 0$			Exponent $n = 1$		
		ϖ_1	ϖ_2	ϖ_3	ϖ_1	ϖ_2	ϖ_3
$u = 0$	Present	21.33	70.41	147.91	34.03	112.33	235.93
	DSM	21.33	70.42	147.90	34.03	112.32	235.94
	Error (%)	0.00	0.01	0.01	0.00	0.01	0.00
	FEM	21.33	70.42	147.91	34.02	112.33	235.94
	Error (%)	0.00	0.01	0.00	0.03	0.00	0.00
$u = 1.5$	Present	20.24	69.52	147.04	33.32	111.74	235.36
	DSM	20.24	69.52	147.03	33.31	111.75	235.37
	Error (%)	0.00	0.00	0.01	0.03	0.01	0.00
	FEM	20.43	69.39	146.82	33.45	111.66	235.23
	Error (%)	0.94	0.19	0.15	0.39	0.07	0.06

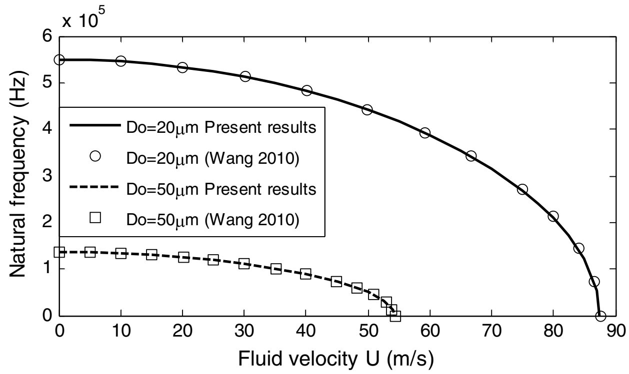

Fig. 6 Comparisons of fundamental natural frequencies of a simply supported micropipe conveying fluid

Figure 6 shows the comparisons of fundamental natural frequencies of a simply supported micropipe conveying fluid with different diameters of the micropipe. It should be noted that the natural frequencies are dimensional in the existing literature (Wang 2010). Therefore, the current study also adopts the dimensional results. The present natural frequencies are compared with the results obtained by DQM (Wang 2010). A very close agreement can be observed between the two results, for both the cases of D_o = 20 μm and D_o = 50 μm. Those results demonstrate that the present hybrid method is accurate for determining the natural frequency of micropipes conveying fluid. In addition, since the lower computational cost of present method has been illustrated detailedly in previous papers (Deng et al. 2017a, b; Guo and Chen 2007), it will not be discussed here for conciseness.

5.2 Free vibration and stability of a multi-span FGM micropipe conveying fluid

In what follows, the investigation is carried out to study the effects of length scale parameter, volume fraction exponent, location and number of supports on the free vibration and stability of the FGM micropipe conveying fluid. In this paper, the outer surface of the FGM pipe is pure alumina, while the inner surface is pure aluminum. And the mechanical properties of constituent materials are expressed in Table 3. The density of the fluid is 1000 kg/m^3. To investigate the size effect, the length scale parameter l of the FGM micropipe is assumed to be 15 μm in the following examples (Ansari et al. 2015; Ke et al. 2012; Salamat-talab et al. 2012; Simsek and Reddy 2013). The current paper will not focus on how to obtain the value of length scale parameter l, and the interested reader can refer to Lam et al. (2003) and Nikolov et al. (2007).

Table 3 Material properties of the FGM micropipe (Salamat-talab et al. 2012)

Materials	E (GPa)	ρ_p (kg/m^3)	ν	L (μm)
Aluminum	70	2700	0.23	15
Alumina	380	3800	0.23	15

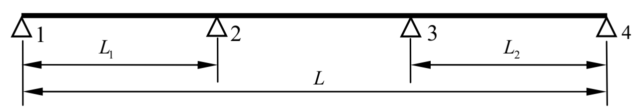

Fig. 7 A three-span FGM micropipe conveying fluid

A representative three-span FGM micropipe conveying fluid is shown in Fig. 7, and the whole pipe is simply supported by four hinged joints. The geometrical parameters of the FGM micropipe are given as $D_i/D_o = 0.9$, $L_1 = L_2 = L/3$ and L/D_o = 20. To investigate the effect of length scale parameter on free vibration and stability of micropipe conveying fluid, the diameter of the micropipe is taken as variable for various values of the ratio of diameter to material length scale parameter D_o/l (dimensionless length scale parameter). It should be mentioned that since the FGM micropipe is homogeneous in axial direction, each span is only need one element in calculation.

For the sake of generality and simplicity, several nondimensional quantities are introduced (Païdoussis 2014)

$$\xi = \frac{x}{L}, \quad u = \left(\frac{M_f}{EI}\right)^{1/2} LU, \quad \varpi = \left(\frac{M_f + m}{EI}\right)^{1/2} \omega L^2 \tag{67}$$

where ξ is the dimensionless length, u the dimensionless fluid velocity and ϖ the dimensionless natural frequency. In order to make the comparison, parameters EI and m in above equation denote flexural rigidity and mass of per unit length of the FGM pipe for exponent $n = 0$.

To investigate the effect of length scale parameter on free vibration and stability of micropipe conveying fluid, the dimensionless fundamental natural frequencies versus dimensionless fluid velocity u with different dimensionless length scale parameters D_o/l are plotted in Fig. 8, and the dimensionless critical velocities for different D_o/l are listed in Table 4. It should be mentioned that the real component of natural frequency, Re(ϖ), is the oscillation frequency, while the imaginary component, Im(ϖ), is related to exponential growth or decay. It has been demonstrated that the real components decrease with the increase in fluid velocity u and the imaginary components keep zero in stable region. When the fluid velocity exceeds a certain value, the real part of natural frequency of first mode becomes

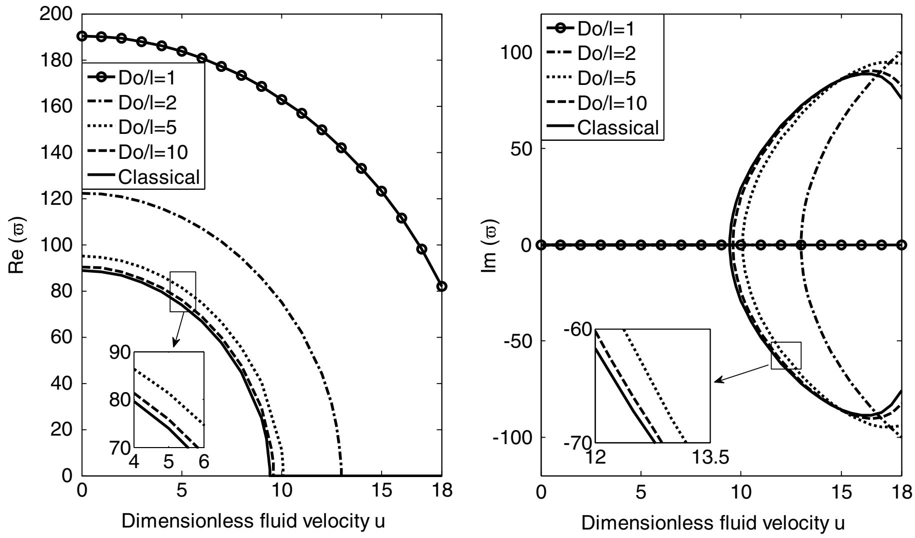

Fig. 8 Fundamental natural frequencies versus fluid velocity u with different D_o/l ($n = 0$)

Table 4 Dimensionless critical velocities for different D_o/l ($n = 0$)

Critical velocity	$D_o/l = 1$	$D_o/l = 2$	$D_o/l = 5$	$D_o/l = 10$	Classical
u_d	20.20	12.99	10.08	9.59	9.43

zero and the imaginary part is negative. This indicates that the pipe loses its stability due to divergence and the corresponding velocity is the critical velocity u_d. It is observed from Fig. 8 and Table 4 that the natural frequencies and critical velocities obtained from the modified couple stress theory are generally higher than those predicted by classical theory. It is also found that the differences between the results calculated by modified couple stress theory and those obtained by classical theory decrease as the increase in dimensionless length scale parameter D_o/l. For example, the critical velocity predicted by modified couple stress theory is about 2.14 times greater than that obtained by the classical beam theory when the dimensionless length scale parameter $D_o/l = 1$. And when the dimensionless parameter $D_o/l = 10$, the ratio of critical velocity determined by modified couple stress theory to classical result reduces to 1.02. It can be concluded that the effect of material length scale parameter on free vibration and stability of micropipe conveying fluid is significant, and it makes the micropipe conveying fluid more stable, especially when the diameter of the micropipe is comparable to the material length scale parameter. This is because that the length scale parameter has the effect of increasing the equivalent bending stiffness $[(EI)^* + (\mu A)^* l^2]$. However, for higher values of $D_o/l (D_o/l > 10)$, the natural frequencies and critical velocities obtained by the modified couple stress theory converge to the classical results.

To study the effect of volume fraction exponent n on free vibration and stability of FGM micropipes conveying fluid, the first three dimensionless natural frequencies of the FGM ($n = 0$, 1, 10) micropipe ($D_o/l = 10$) as functions of dimensionless fluid velocity u are shown in Fig. 9. It can be seen from Fig. 9a that the FGM micropipe displays some more complex and interesting dynamic behaviors when the exponent $n = 0$. Specifically, the divergence of first mode occurs at $u = 9.59$, the divergence of the second mode occurs at $u = 11.78$, and the divergence occurs in third mode at $u = 15.69$. Subsequently, it is of interest to note that as the fluid velocity increases to 17.60, the combination of second and third modes occurs, the real parts are positive, and the imaginary components are negative. This implies the multi-span micropipe loses its stability by coupled-mode flutter, and the corresponding velocity is flutter velocity u_f. It should be stressed that the coupled-mode flutter in single-span pipe conveying fluid is composed by first and second modes firstly. In this study, the coupled-mode flutter occurs in second and third modes directly, which is different from the single-span pipe conveying fluid. It is also found that the real components and the critical velocities increase with the increase in volume fraction exponent n. When the exponent $n = 1$, the divergence of the first mode occurs at $u = 17.50$. And when the exponent $n = 10$, the divergence does not occur in the range of fluid velocity $u < 18$. Therefore, it can be concluded that the stability of the FGM micropipe increases with the increase in volume fraction exponent n. This is due to the fact that the content of alumina in FGM pipe increases, while the content of aluminum decreases with increasing exponent n, and the Young's modulus of the alumina is much larger than that of aluminum. More interestingly, it is found that distributions of natural frequencies of the FGM micropipe can be adjusted easily by designing the exponent n. For instance, when the fluid velocity $u = 0$, the first-order natural frequency for exponent $n = 10$ is about 2.11 times greater than that of exponent $n = 0$. Therefore, if the dominant

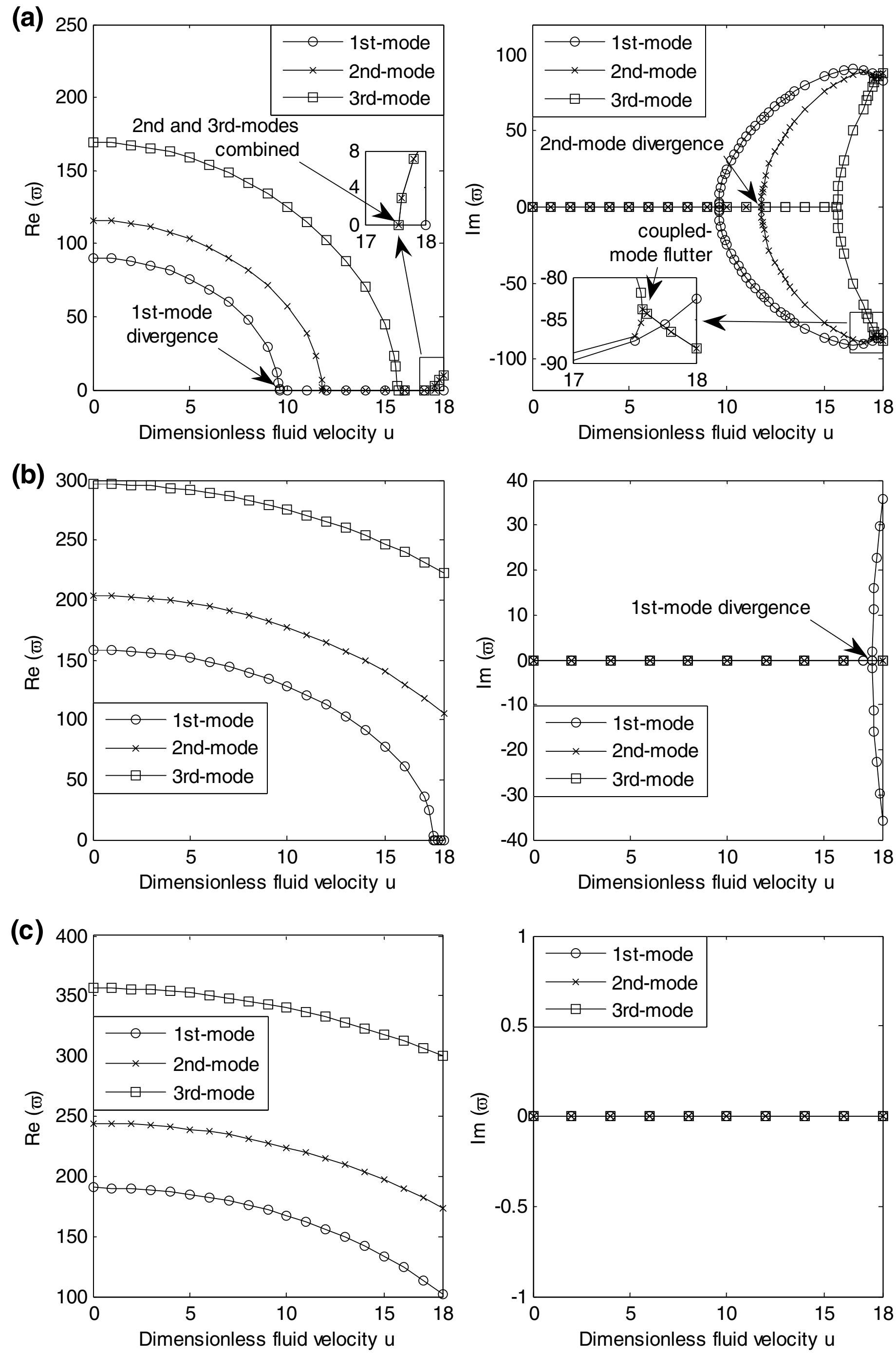

Fig. 9 First three natural frequencies of FGM micropipe conveying fluid against fluid velocity u ($D_o/l = 10$): **a** exponent $n = 0$, **b** exponent $n = 1$, **c** exponent $n = 10$

frequency contents of external loads are known, a proper design for FGM micropipe to avoid the resonance to reduce the vibration is possible.

To further examine the effects of volume fraction exponent n and dimensionless length scale parameter D_o/l on stability of the FGM micropipe conveying fluid, critical velocities versus exponent n with different dimensionless length scale parameters ($D_o/l = 1, 2, 5, 10$) are shown in Fig. 10a, and the results determined by the classical FGM beam model ($l = 0$) are also given in Fig. 10a. Critical velocities against dimensionless length scale parameter D_o/l with different exponents n ($n = 0, 1, 10$) are shown in Fig. 10b. It is clear from Fig. 10a that the critical velocities predicted by the modified couple stress theory are larger than those obtained by classical beam theory. This is because that the size effect increases the stiffness of the micropipe. With the increase in D_o/l from 1 to 10, the critical velocities decrease significantly, and the difference

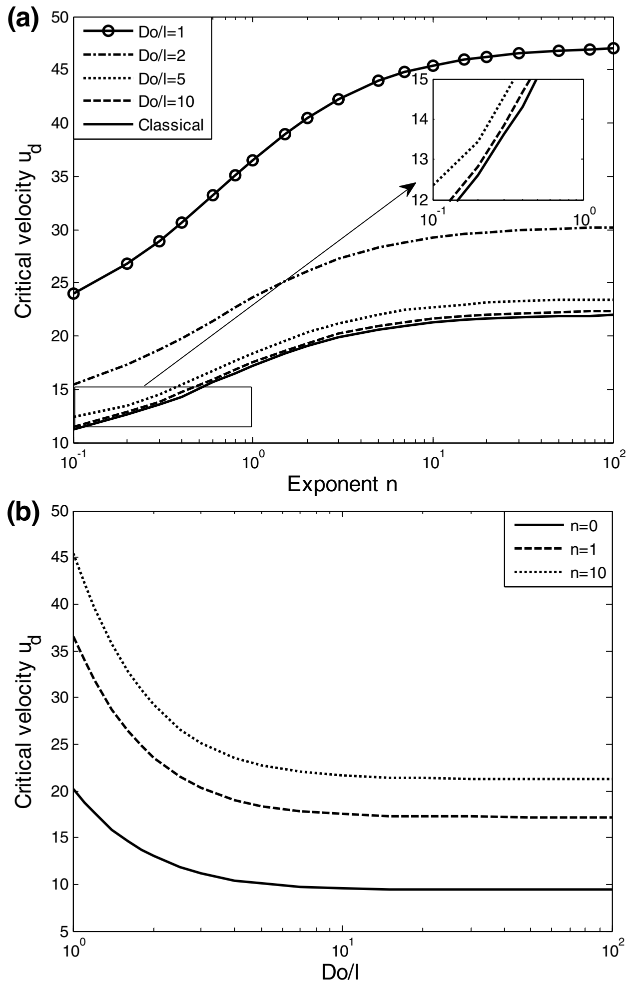

Fig. 10 Effects of exponent n and parameter D_o/l on critical velocity: **a** Critical velocity u_d against D_o/l with different exponents n; **b** critical velocity u_d against exponent n with different D_o/l

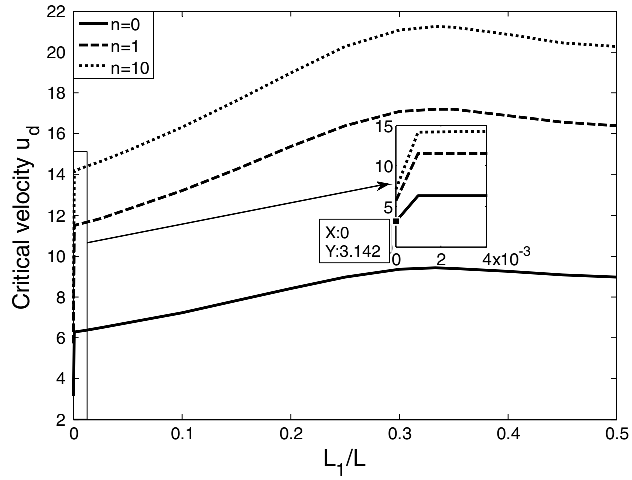

Fig. 11 Critical velocity u_d against dimensionless length of L_1/L with different exponents n ($D_o/l = 100$)

between the critical velocities of modified couple stress theory and classical ones diminishes gradually. It can be seen from Fig. 10b that the critical velocities decrease with the increase in dimensionless length scale parameter D_o/l, and when the parameter $D_o/l > 10$, the critical velocities gradually approach to constants. The reason is that the introduction of couple stress stiffens the micropipe and the size effect is significantly only when the diameter of micropipe is comparable to the length scale parameter. For higher values of D_o/l ($D_o/l > 10$), the results predicted by modified couple stress theory converge to the classical ones. On the other hand, it can be found from Fig. 10a that the critical velocities increase with the increase in exponent n; especially, the critical velocities increase rapidly when the exponent n is less than 10. As the exponent n increases further, the effect on the critical velocities becomes less pronounced. And when the exponent $n > 50$, the critical velocities gradually approach to constants. This is reasonable because a little change of exponent n could increase the volume fraction of alumina markedly when the exponent $n < 10$, and the Young's modulus of the alumina is much larger than that of aluminum. When the exponent $n > 10$, the variation of volume fraction in FGM pipe for different exponents becomes slow. When the exponent $n > 50$, FGM micropipe has approached to the alumina micropipe. Those results provide useful information for designers to choose reasonable values of dimensionless length scale parameter and volume fraction exponent to improve the stability of FGM micropipe conveying fluid.

In practical engineering applications, the location of intermediate supports is always constrained by surrounding situations, and the intermediate supports cannot be evenly distributed in piping systems. Therefore, it is necessary to investigate the effect of location of supports on stability of multi-span micropipe conveying fluid. In this case, the supports 2 and 3 in Fig. 7 simultaneously move from left and right sides to middle point, respectively ($0 \le L_1 = L_2 \le L/2$). The critical velocities versus dimensionless length of L_1/L with different exponents n ($n = 0, 1, 10$) are plotted in Fig. 11. It can be seen from Fig. 11 that when the dimensionless length of $L_1/L = 0$ and parameter $D_o/l = 100$, the critical velocity for exponent $n = 0$ is $3.142 \approx \pi$ (π is the exact critical velocity for a pinned–pinned pipe conveying fluid). Actually, when the length of $L_1 = L_2 = 0$ and exponent $n = 0$, the three-span FGM micropipe degenerates to a single-span homogeneous micropipe, and the parameter $D_o/l = 100$ implies that the critical velocity predicted by modified couple stress theory has converged to the classical result. Therefore, the critical velocity 3.142 obtained by present method shows good agreement with the exact solution (Païdoussis 2014). As is observed in Fig. 11, when the dimensionless length of

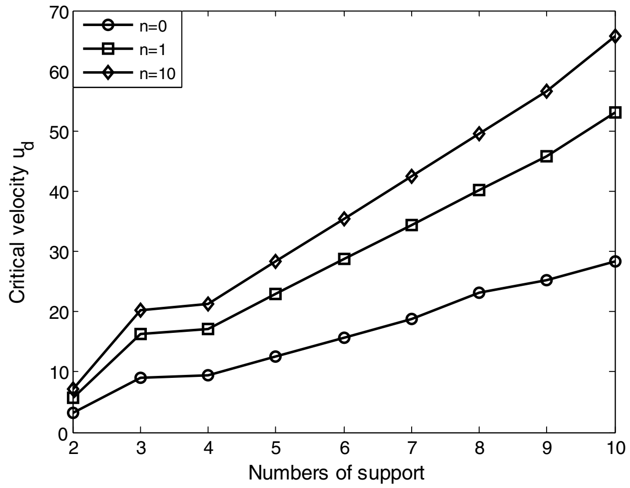

Fig. 12 Critical velocity u_d against numbers of support with different exponents n ($D_o/l = 100$)

L_1/L is about 0.33, there are maximum critical velocities. This is reasonable because the three-span pipe has maximum stiffness when the supports are evenly distributed in piping system. It also can be seen that the critical velocities have sharp increases when the dimensionless length L_1/L changes from 0 to a small value. This implies that the stiffness has a sharp increase when the intermediate supports are mounted in the single-span pipe.

To investigate the number of support on stability of multi-span FGM micropipes conveying fluid, the critical velocities against numbers of support are plotted in Fig. 12. In this case, the supports are evenly distributed in the piping system. Generally, with the increase in number of supports, the critical velocities increase linearly when the number is less than 10. It is also interesting to note that the critical velocities have sharp increases when the single-span micropipe changes to the two-span micropipe conveying fluid, and the increments of critical velocity are not obvious when the piping system changes from two-span micropipe to three-span micropipe. In general, the intermediate supports can significantly increase the stiffness and expand the stability region of micropipe conveying fluid. These results may provide a reference to application and design of multi-span pipe conveying fluid.

6 Conclusions

In this paper, the size-dependent free vibration and stability of multi-span FGM micropipes conveying fluid are investigated. Equations of motion are established by applying the modified couple stress theory and the Hamilton's principle. Then, a hybrid method which combines the MRRM and the wave propagation method is developed to determine the natural frequencies. Some main conclusions obtained from the results are presented as follows:

1. The results demonstrate that present hybrid method is especially suitable for dynamic analysis of multi-pipes conveying fluid with high accuracy by using only a small number of elements.
2. The size effect is significant when the diameter of the micropipe is comparable to the length scale parameter and it makes the micropipe conveying fluid more stable.
3. Natural frequencies and critical velocities increase rapidly with the increase in exponent n when it is less than 10. And the distributions of natural frequencies also can be adjusted easily by designing the exponent n.
4. The intermediate supports could improve the stability of pipe conveying fluid considerably, and it also enriches the dynamic behavior of pipe conveying fluid, specifically by revealing that the coupled-mode flutter occurs in second and third modes directly, which has not been observed in single-span pipe conveying fluid.

Acknowledgements This project is supported by National Natural Science Foundation of China (Grant Number 51305350) and the Basic Researches Foundation of NWPU (Grant Number 3102014JCQ01045).

References

Aghazadeh R, Cigeroglu E, Dag S (2014) Static and free vibration analyses of small-scale functionally graded beams possessing a variable length scale parameter using different beam theories. Eur J Mech A–Solid 46:1–11

Amiri A, Pournaki IJ, Jafarzadeh E, Shabani R, Rezazadeh G (2016) Vibration and instability of fluid-conveyed smart micro-tubes based on magneto-electro-elasticity beam model. Microfluid Nanofluid. doi:10.1007/s10404-016-1706-5

Ansari R, Gholami R, Norouzzadeh A, Sahmani S (2015) Size-dependent vibration and instability of fluid-conveying functionally graded microshells based on the modified couple stress theory. Microfluid Nanofluid 19:509–522

Ansari R, Gholami R, Norouzzadeh A (2016a) Size-dependent thermo-mechanical vibration and instability of conveying fluid functionally graded nanoshells based on Mindlin's strain gradient theory. Thin Wall Struct 105:172–184

Ansari R, Norouzzadeh A, Gholami R, Shojaei MF, Darabi MA (2016b) Geometrically nonlinear free vibration and instability of fluid-conveying nanoscale pipes including surface stress effects. Microfluid Nanofluid. doi:10.1007/s10404-015-1669-y

Asghari M, Ahmadian MT, Kahrobaiyan MH, Rahaeifard M (2010) On the size-dependent behavior of functionally graded micro-beams. Mater Des 31:2324–2329

Birman V, Byrd LW (2007) Modeling and analysis of functionally graded materials and structures. Appl Mech Rev 60:195–216

Chen A, Su J (2017) Dynamic behavior of axially functionally graded pipes conveying fluid. Math Probl Eng. doi:10.1155/2017/6789634

Deng JQ, Liu YS, Zhang ZJ, Liu W (2016) Dynamic behaviors of multi-span viscoelastic functionally graded material pipe conveying fluid. Proc Inst Mech Eng Part C J Mech Eng Sci. doi:10.1177/0954406216642483

Deng JQ, Liu YS, Zhang ZJ, Liu W (2017a) Stability analysis of multi-span viscoelastic functionally graded material pipes conveying fluid using a hybrid method. Eur J Mech A–Solid. doi:10.1016/j.euromechsol.2017.04.003

Deng JQ, Liu YS, Liu W (2017b) A hybrid method for transverse vibration of multi-span functionally graded material pipes conveying fluid with various volume fraction laws. Int J Appl Mech (**Accetp**)

Enoksson P, Stemme G, Stemme E (1997) A silicon resonant sensor structure for Coriolis mass-flow measurements. J Microelectromech Syst 6:119–125

Eringen AC (1972) Nonlocal poplar elastic continua. Int J Eng Sci 10(1):1–16

Filiz S, Aydogdu M (2015) Wave propagation analysis of embedded (coupled) functionally graded nanotubes conveying fluid. Compos Struct 132:1260–1273

Fleck NA, Muller GM, Ashby MF, Hutchinson JW (1994) Strain gradient plasticity: theory and experiment. Acta Metall Mater 42:475–487

Fu YQ, Du HJ, Huang WM, Zhang S, Hu M (2004) TiNi-based thin films in MEMS applications: a review. Sens Actuat A-Phys 112:395–408

Guo YQ, Chen WQ (2007) Dynamic analysis of space structures with multiple tuned mass dampers. Eng Struct 29:3390–3403

Guo CQ, Zhang CH, Païdoussis MP (2010) Modification of equation of motion of fluid-conveying pipe for laminar and turbulent flow profiles. J Fluid Struct 26:793–803

Gurtin ME, Murdoch AI (1975) A continuum theory of elastic material surfaces. Arch Ration Mech Anal 57:291–323

Harland NR, Mace BR, Jones RW (2001) Wave propagation, reflection and transmission in tunable fluid-filled beams. J Sound Vib 241(5):735–754

Howard SM, Pao YH (1998) Analysis and experiments on stress waves in planar trusses. J Eng Mech 124:884–891

Ibrahim RA (2010) Overview of mechanics of pipes conveying fluids-Part I: fundamental studies. J Press Vess Technol ASME 132:1–32

Ibrahim RA (2011) Mechanics of pipes conveying fluids-Part II: applications and fluidelastic problems. J Press Vess Technol ASME 133:1–30

Jha DK, Kant T, Singh RK (2013) Critical review of recent research on functionally graded plates. Compos Struct 96:833–849

Ke LL, Wang YS, Yang J, Kitipornchai S (2012) Nonlinear free vibration of size-dependent functionally graded microbeams. Int J Eng Sci 50:256–267

Komijani M, Esfahani SE, Reddy JN, Liu YP, Eslami MR (2014) Nonlinear thermal stability and vibration of pre/post-buckled temperature- and microstructure-dependent functionally graded beams resting on elastic foundation. Compos Struct 112:292–307

Lam DCC, Yang F, Chong ACM, Wang J, Tong P (2003) Experiments and theory in strain gradient elasticity. J Mech Phys Solids 51:1477–1508

Lee Z, Ophus C, Fischer LM, Nelson-Fitzpatrick N, Westra KL, Evoy S, Radmilovic V, Dahmen U, Mitlin D (2006) Metallic NEMS components fabricated from nanocomposite Al–Mo films. Nanotechnology 17(12):3063–3070

Lee SK, Mace BR, Brennan MJ (2007) Wave propagation, reflection and transmission in non-uniform one-dimensional waveguides. J Sound Vib 304:31–49

Li L, Hu YJ (2016a) Wave propagation in fluid-conveying viscoelastic carbon nanotubes based on nonlocal strain gradient theory. Comput Mater Sci 112:282–288

Li L, Hu YJ (2016b) Critical flow velocity of fluid-conveying magneto-electro-elastic pipe resting on an elastic foundation. Int J Mech Sci 119:273–282

Li L, Hu YJ (2017a) Nonlinear bending and free vibration analysis of nonlocal strain gradient beams made of functionally graded material. Int J Eng Sci 107:77–97

Li L, Hu YJ (2017b) Torsional vibration of bi-directional functionally graded nanotubes based on nonlocal elasticity theory. Compos Struct 172:242–250

Li BH, Gao HS, Liu YS, Yue ZF (2012a) Transient response analysis of multi-span pipe conveying fluid. J Vib Control 19(14):2164–2176

Li BH, Gao HS, Liu YS, Yue ZF (2012b) Free vibration analysis of micropipe conveying fluid by wave method. Results Phys 2:104–109

Li SJ, Karney BW, Liu GM (2015) FSI research in pipeline systems—a review of the literature. J Fluid Struct 57:277–297

Li L, Hu YJ, Li XB, Ling L (2016a) Size-dependent effects on critical flow velocity of fluid-conveying microtubes via nonlocal strain gradient theory. Microfluid Nanofluid. doi:10.1007/s10404-016-1739-9

Li L, Li XB, Hu YJ (2016b) Free vibration analysis of nonlocal strain gradient beams made of functionally graded material. Int J Eng Sci 102:77–92

Lim CW, Zhang G, Reddy JN (2015) A higher-order nonlocal elasticity and strain gradient theory and its applications in wave propagation. J Mech Phys Solids 78:298–313

Lü CF, Lim CW, Chen WQ (2009) Size-dependent elastic behavior of FGM ultra-thin films based on generalized refined theory. Int J Solids Struct 46:1176–1185

Ma ZY, Chen JL, Li B, Li Z, Su XY (2016) Dispersion analysis of Lamb waves in composite laminates based on reverberation-ray matrix method. Compos Struct 136:419–429

Miao FX, Sun GJ, Chen KF (2013) Transient response analysis of balanced laminated composite beams by the method of reverberation-ray matrix. Int J Mech Sci 77:121–129

Mindlin RD, Eshel NN (1968) On the first strain-gradient theories in linear elasticity. Int J Solids Struct 4:109–124

Najmzadeh M, Haasl S, Enoksson P (2007) A silicon straight tube fluid density tensor. J Micromech Microeng 17:1657–1663

Nateghi A, Salamat-talab M (2013) Thermal effect on size dependent behavior of functionally graded microbeams based on modified couple stress theory. Compos Struct 96:97–110

Nikolov S, Han CS, Raabe D (2007) On the origin of size effects in small-strain elasticity of solid polymers. Int J Solids Struct 44:1582–1592

Païdoussis MP (2014) Fluid-structure interactions: slender structures and axial flow, vol 1, 2nd edn. Academic Press, New York

Païdoussis MP, Li X (1993) Pipes conveying fluid: a model dynamical problem. J Fluid Struct 7:137–204

Pao YH, Chen WQ (2009) Elastodynamic theory of framed structures and reverberation-ray matrix analysis. Acta Mech 204:61–79

Pao YH, Keh DC, Howard SM (1999) Dynamic response and wave propagation in plane trusses and frames. AIAA J 37:594–603

Reddy JN (2011) Microstructure-dependent couple stress theories of functionally graded beams. J Mech Phys Solids 59:2382–2399

Rinaldi S, Prabhakar S, Vengallatore S, Païdoussis MP (2010) Dynamics of microscale pipes containing internal fluid flow: damping, frequency shift, and stability. J Sound Vib 329:1081–1088

Salamat-talab M, Nateghi A, Torabi J (2012) Static and dynamic analysis of third-order shear deformation FG micro beam based on modified couple stress theory. Int J Mech Sci 57:63–73

Setoodeh AR, Afrahim S (2014) Nonlinear dynamic analysis of FG micro-pipes conveying fluid based on strain gradient theory. Compos Struct 116:128–135

Shen Y, Chen YJ, Li L (2016) Torsion of a functionally graded material. Int J Eng Sci 109:14–28
Sheng GG, Wang X (2008) Thermomechanical vibration analysis of a functionally graded shell with flowing fluid. Eur J Mech A–Solids 27:1075–1087
Sheng GG, Wang X (2010) Dynamic characteristics of fluid-conveying functionally graded cylindrical shells under mechanical and thermal loads. Compos Struct 93:162–170
Simsek M, Reddy JN (2013) Bending and vibration of functionally graded microbeams using a new higher order beam theory and the modified couple stress theory. Int J Eng Sci 64:37–53
Tan CA, Kang B (1998) Wave reflection and transmission in an axially strained, rotating Timoshenko shaft. J Sound Vib 231(3):483–510
Tian JY, Xie ZM (2009) A hybrid method for transient wave propagation in a multilayered solid. J Sound Vib 325:161–173
Toupin RA (1962) Elastic materials with couple-stresses. Arch Ration Mech Anal 11:385–414
Wang L (2010) Size-dependent vibration characteristics of fluid-conveying microtubes. J Fluid Struct 26:675–684
Wang ZM, Liu YZ (2016) Transverse vibration of pipe conveying fluid made of functionally graded materials using a symplectic method. Nucl Eng Des 289:149–159
Wang YQ, Zu JW (2017) Nonlinear steady-state responses of longitudinally traveling functionally graded material plates in contact with liquid. Compos Struct 164:130–144
Wang L, Dai HL, Qian Q (2012) Dynamics of simply supported fluid-conveying pipes with geometric imperfections. J Fluid Struct 7:137–204
Wang L, Liu HT, Ni Q, Wu Y (2013) Flexural vibrations of microscale pipes conveying fluid by considering the size effects of micro-flow and micro-structure. Int J Eng Sci 71:92–101
Wu JS, Shih PY (2001) The dynamic analysis of a multispan fluid conveying pipe subjected to external load. J Sound Vib 239(2):201–215
Wu ZJ, Luo Z, Rastogia A, Stavchansky S, Bowman PD, Ho PS (2011) Micro-fabricated perforated polymer devices for long-term drug delivery. Biomed Microdevices 13:485–491
Yang F, Chong ACM, Lam DCC, Tong P (2002) Couple stress based strain gradient theory for elasticity. Int J Solids Struct 39:2731–2743
Yang TZ, Ji SD, Yang XD, Fang B (2014) Microfluid-induced nonlinear free vibration of microtubes. Int J Eng Sci 76:47–55
Zhang XM (2002) Parametric studies of coupled vibration of cylindrical pipes conveying fluid with the wave propagation approach. Comput Struct 80:287–295
Zhang YW, Yang TZ, Zang J, Fang B (2013) Terahertz wave propagation in a nanotube conveying fluid taking into account surface effect. Materials 6:2393–2399
Zhang ZJ, Liu YS, Li BH (2014) Free vibration analysis of fluid-conveying carbon nanotube via wave method. Acta Mech Solida Sin 27:626–634
Zhang YW, Yang TZ, Zang J, Zeng W, Fang B (2015) Thermal effect on terahertz wave propagations in nanotube conveying fluid. Mater Res Innov 19:570–573